Geoderma 314 (2018) 245–261

Contents lists available at ScienceDirect

Geoderma

journal homepage: www.elsevier.com/locate/geoderma

Climate, topography, and dust influences on the mineral and geochemical evolution of granitic soils in southern Arizona

Rebecca A. Lybrand*, Craig Rasmussen

Department of Soil, Water and Environmental Science, University of Arizona, Tucson, AZ, 85721, USA

ARTICLE INFO

Editor: M. Vepraskas

ABSTRACT

Mineral weathering transforms rock into soils that supply nutrients to ecosystems, store terrestrial carbon, and provide habitat for organisms. As a result, the mineralogy and geochemistry of soils from contrasting environments are well-studied. The primary objective of this research was to examine how climate, topography, and dust interactively control the mineral and geochemical composition of granitic soils that span an environmental gradient in southern Arizona. Two field sites were selected within the Catalina Critical Zone Observatory that exhibit significant range in precipitation (25 to 85 cm yr^{-1}), temperature (24 to 10 °C), and vegetation composition (desert scrub → mixed conifer). Within each site, two *catena* end member pairs were selected to represent variation in local topography which included divergent, water-shedding summits and convergent, water-gathering footslopes. Soils and parent rock were studied using x-ray diffraction and x-ray fluorescence. Dust samples were collected from ridgetop dust traps at the desert scrub site and examined using x-ray fluorescence. The desert scrub soils showed enrichment in biotite, total feldspar, and Fe + Mg whereas the mixed conifer soils were depleted in feldspars and enriched in Fe + Mg. Depletions of Na, Si, and K + Ca occurred in both the desert and mixed conifer ecosystems, with the convergent soils in the conifer sites exhibiting the greatest degree of elemental loss. We examined dust in the regolith after identifying mineral and elemental enrichments in both ecosystems. Dust fraction estimates ranged from 2 to 21% in desert soils and 9 to 19% for the mixed conifer soils. Our results confirm the interactive role of bioclimate, topography, and dust in driving the geochemical evolution of soils and cycling of nutrients in desert and conifer ecosystems.

1. Introduction

Mineral weathering serves a fundamental role in the critical zone by transforming bedrock to a mantle of weathered rock and soil that delivers nutrients to ecosystems; stores and partitions water; and shapes climate change feedbacks with the global carbon cycle (Berner et al., 1983; White and Brantley, 1995; Dixon et al., 2009). The weathering of silicate minerals, in particular, leads to the retention of atmospherically derived carbon in soils and sediments over geologic timescales (Goudie and Viles, 2012), making the controls on silicate weathering a subject of much study (e.g., Dahlgren et al., 1997; Riebe et al., 2001, 2004; West et al., 2005; Rasmussen et al., 2011). Questions remain on the mechanisms that define climate-weathering relationships across landscapes (Dixon et al., 2012) and how tectonic, topographic, and biologic factors interact as drivers in silicate weathering processes (West et al., 2005). Here, we ask how climate, vegetation, and landscape position drive the weathering of silicate minerals in granitic soils that span desert to mixed conifer ecosystems in southern Arizona. We also assess the role of external dust inputs in soil development across these systems.

The weathering of primary minerals in granitic terrain leads to elemental losses that generally intensify in wetter climates (Whittaker et al., 1968; Dahlgren et al., 1997; Bockheim et al., 2000; Egli et al., 2003; Khomo et al., 2013) and in downslope, water-gathering landscape positions (Nettleton et al., 1968; Hattar et al., 2010; Khomo et al., 2011). Hillslope steepness and landscape stability complicate these climate-landscape relationships that are associated with moisture availability. One such example occurs in the San Gabriel Mountains, California where low-gradient hillslopes (< 25°) exhibited different chemical weathering properties than high-gradient hillslopes (> 25°) in otherwise similar weathering environments (Dixon et al., 2012). Chemical weathering, as quantified by chemical depletion fractions (CDF) and tau values, was greatest in downslope positions of low-gradient hillslopes as would be expected given the conventional *catena* model (Huggett, 1975; Sommer and Schlichting, 1997; Birkeland, 1999). Conversely, in the 20–30° transition to high-gradient hillslopes, chemical depletion decreased downslope; a finding linked to kinetic

* Corresponding author at: Department of Crop and Soil Science, Oregon State University, Corvallis, OR 97331, USA.
E-mail addresses: Rebecca.Lybrand@oregonstate.edu (R.A. Lybrand), crasmuss@cals.arizona.edu (C. Rasmussen).

https://doi.org/10.1016/j.geoderma.2017.10.042
Received 29 July 2017; Received in revised form 18 October 2017; Accepted 22 October 2017
Available online 06 December 2017

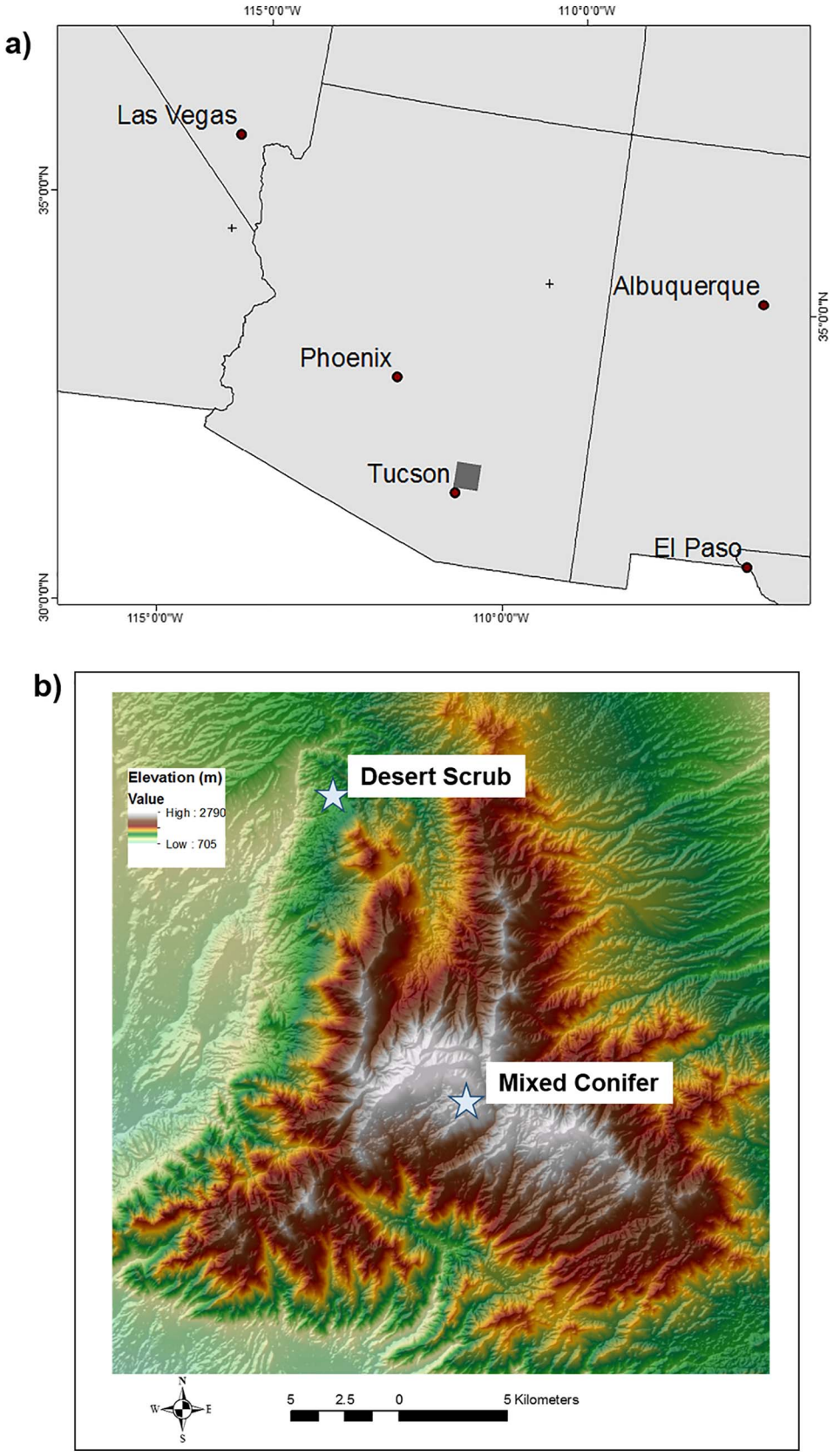

Fig. 1. Site maps for the Catalina Critical Zone Observatory (CZO) including a) an inset map of the CZO located in southern Arizona and b) a digital elevation map showing the desert scrub and mixed conifer field sites.

controls on mineral weathering in tectonically active landscapes that results in greater physical erosion rates, shallow soils, and shorter soil mean residence times compared to low-gradient hillslopes (Dixon et al., 2012). Studies of mineral weathering along hillslopes require consideration of soils with relatively short residence times that integrate estimates of physical erosion rates and the degree of geomorphic stability (Yoo et al., 2007; Dixon et al., 2012). Furthermore, the products of weathering illustrate regional to local site properties,

Table 1
Field site characteristics for the desert scrub and mixed conifer soils in the Catalina Critical Zone Observatory. Site characteristics include mean annual temperature (MAT), mean annual precipitation (MAP), and major overstory vegetation type. Climate, vegetation, and geology data were published previously for the desert scrub and mixed conifer sites (Lybrand and Rasmussen, 2014; Lybrand and Rasmussen, 2015).

Field site	Elevation (m)	MAT (°C)	MAP (cm)	MAP/PET ratio	Parent rock	Dominant vegetation type
Desert scrub	1092	18	45	0.53	Catalina granitic pluton (Oligocene-Miocene)	Saguaro (*Carnegiea gigantean*), Ocotillo (*Fouquieria splendens*), Acacia, Arizona Barrel Cactus (*Ferocactus wislizeni*), and Agave (*Agave schotti*, *Agave palmeri*)
Mixed conifer	2408	9.4	95	1.47	Wilderness granite suite (two-mica granite; Eocene)	Douglas fir (*Pseudotsuga menziesii*), Ponderosa Pine (*Pinus ponderosa*) and White fir (*Abies concolor*)

including clay minerals that vary in composition and abundance as a function of moisture availability and temperature (Barshad, 1966; Berry, 1987; Khomo et al., 2011).

Clay minerals provide insight into climate and localized hydrological conditions in the soil environment (Turpault et al., 2008; Sandler, 2013). Smectite generally dominates the clay mineral fraction in hot, water-limited desert environments, and can co-occur with kaolinite, vermiculite, and palygorskite (Nettleton et al., 1968; Graham and O'Geen, 2010; Khomo et al., 2011). Kaolinite, hydroxyl-interlayered minerals, gibbsite, and short range-ordered minerals can comprise the clay fractions of wetter, cooler environments. Kaolinite is ubiquitous across climatic regimes whereas halloysite, an intermediate weathering product in the transformation of plagioclase to kaolinite (Joussein et al., 2005), predominates in volcanically derived soils (Parfitt et al., 1983; Southard and Southard, 1987) or soils formed in humid, wet climates (Jeong, 2000). Halloysite has also been documented in arid environments with rapid soil drying that kinetically limits the formation of smectite (Ziegler et al., 2003). Climate-landscape relationships explain clay mineral type and abundance as demonstrated along a series of arid to sub-humid granitic catenas in South Africa, where the proportion of kaolinite to smectite increased in both wetter landscape positions and higher rainfall regions (Khomo et al., 2011). The study of clay minerals along bioclimate and topographic gradients demonstrate moisture-driven controls on in situ mineral weathering, yet the role of dust-derived minerals is less well-understood.

Fine-grained dust inputs provide a critical medium for plant growth, in the form of nutrients and increased water holding capacities, in otherwise inhospitable or nutrient-limited terrain (Muhs et al., 2008). Eolian dust deposition represents a fundamental geomorphic process that contributes to soil formation and its associated geochemistry in landscapes spanning arid (Wells et al., 1985; Reheis et al., 1995; Reheis, 2006; Reynolds et al., 2006; Crouvi et al., 2013; Sandler, 2013) to alpine ecosystems (Litaor, 1987; Bockheim and Koerner, 1997; Muhs and Benedict, 2006; Rasmussen et al., 2017), yet the role of dust deposition is still underrepresented in the literature (McTainsh and Strong, 2007). Silt-enriched soil mantles observed across desert and high-elevation environments are attributed to dust accretion over modern and/or geologic time (Wells et al., 1985; Dahms, 1993; Bockheim and Koerner, 1997; Muhs and Benedict, 2006). Dust fraction estimates were up to four times greater at hillslope bases compared to ridge top summits in the Mojave soils (Crouvi et al., 2013), indicating an important geomorphic consideration on the distribution of dust. Dust composition, transport distance, and origin (e.g., playas, alluvial deposits, and sites of anthropogenic disturbance) vary by location (Muhs and Benedict, 2006; Bullard et al., 2011; Hirmas and Graham, 2011).

The primary goal of this study was to examine bioclimate and hillslope scale controls on mineral weathering along an environmental gradient in Arizona that encompasses semiarid to subhumid ecosystems. We identified primary and secondary mineral composition, quantified primary mineral abundance in soils, and calculated bulk soil elemental losses and gains for climate and hillslope end members in the Catalina Critical Zone Observatory. The elemental ratios of dust, soil, and rock samples were determined to better understand dust fraction inputs to the landscapes. We hypothesized that the thin, weakly developed soils in the desert system comprise substantial inputs of dust with minerals that would show variable degrees of transformation given the mix of potential dust sources in the area. More in situ mineral weathering was expected for the mixed conifer system where increased precipitation and productivity contribute to deeper soils that would dilute external dust imprints.

2. Methods

Soil, rock, and dust samples were collected from north-facing granitic hillslopes in the Santa Catalina Mountain Critical Zone Observatory (SCM-CZO) that span two climate-vegetation zones, referred to herein as desert scrub and mixed conifer (Fig. 1a,b). Mean annual temperature (MAT), mean annual precipitation (MAP), elevation, parent rock type, and dominant vegetation for each site are summarized in Table 1. Within each climate-vegetation zone, samples were collected from two divergent summit and two convergent footslope positions to account for topographic controls on mineral transformation. Divergent positions shed water, soil materials, and solutes downslope to convergent footslopes where greater moisture availability results in enhanced mineral weathering. The field experiment design follows similar hillslope scale soil studies that focus on the interactive control of climate and topography on granitic soil development (Watson, 1964; Muhs, 1982; Khomo et al., 2011). The desert scrub and mixed conifer locations represent the two bioclimatic end members of the environmental gradient (e.g., Whittaker and Niering, 1965; Whittaker et al., 1968), with sites selected based on the well-constrained geology of the field areas (Dickinson, 1991,2002).

All soils were air-dried, and sieved at < 2 mm to isolate the "fine-earth" fraction for analysis (Soil Survey Staff, 2004). Major, minor, and trace elemental constituents were determined by x-ray fluorescence (XRF) for all soil and rock samples. Soils were prepared by ball milling ~3.5 g of sample in a plastic scintillation vial containing 3 tungsten carbide bearings for 10 min. Internal rock fragments were ground to < 355 μm using a porcelain mortar and pestle. The ground soil and rock samples were formed into pellets under a pressure of 25 tons for 120 s, bound with cellulose wax (3642 Cellulose binder – SPEX SamplePrep PrepAidTM), and analyzed using a Polarized Energy-Dispersive X-ray Fluorescence spectrometer (EDXRF – SPECTRO XEPOS, Kleve – Germany). The XRF concentrations measured for soils were corrected for loss on ignition and reported on an ash free basis. Loss on ignition was determined by weighing out 20 g of dried (105 °C for 24 h), untreated soil, placing the sample in a muffle furnace for 3 h at 550 °C, cooling the sample in a desiccator, and re-weighing the sample post-ignition. Loss on ignition was then calculated as the percent of dry weight that was lost on ignition (Konen et al., 2002).

Elemental and mineralogical mass transfers were calculated using Zr and quartz as the respective immobile constituents. Mobile elemental constituents included Na, Si, K + Ca, Fe + Mg, and Al. Mobile mineral constituents included biotite, oligoclase, and orthoclase for the desert soils whereas muscovite (and to a lesser degree, biotite), oligoclase, and microcline comprised the dominant mineral constituents in the mixed

Table 2
A summary of the mineral assemblage and associated weight percentages (± 1σ) for the desert scrub and mixed conifer soils. The mineral weight percentages are presented as averages for all soil horizon samples from 2 pedons examined for each landscape position type. The number of soils included in each average are as follows: $n = 8$ and $n = 13$ samples from the respective divergent and convergent landscape positions in the mixed conifer system. The number of soil samples for the desert scrub sites include $n = 6$ and $n = 8$ for the divergent and convergent positions, respectively.

Ecosystem	Landscape position	Quartz (%)	Na-Feldspar (%)	K-Feldspar (%)	Mica (%)
Mixed conifer	Divergent	30 ± 2.2	36 ± 2.0[a]	19 ± 1.1[b]	14 ± 1.9[d]
	Convergent	35 ± 2.2	32 ± 1.1[a]	19 ± 0.5[b]	14 ± 1.7[d]
Desert scrub	Divergent	27 ± 2.5	44 ± 2.3[a]	22 ± 2.1[c]	7 ± 1.1[e]
	Convergent	28 ± 1.7	43 ± 4.1[a]	22 ± 3.0[c]	7 ± 2.0[e]

Symbols indicate dominant mineral species for each ecosystem.
[a] Oligoclase.
[b] Microcline.
[c] Orthoclase.
[d] Biotite/Muscovite.
[e] Biotite.

conifer soils as identified in prior work (Lybrand and Rasmussen, 2014). The mass transfers were calculated using the dimensionless mass transfer coefficient, $\tau_{i,j}$, following Porder et al. (2007):

$$\tau_{i,j} = \left[\frac{c_{j,w}}{c_{j,p}}\frac{c_{i,p}}{c_{i,w}} - 1\right] \times [1 - RF\%] \quad (1)$$

where $c_{j,p}$ and ci,p are concentrations of the mobile and immobile constituents in the parent material, $c_{j,w}$ and $c_{i,w}$ are soil concentrations, and RF% is weight percent rock fragments.

Dust samples were collected in 2012 from four dust traps deployed for 1 year along a ridge top at the desert scrub location. The dust traps were similar in construction to those described by Reheis and Kihl (1995). The samples were prepared and analyzed using the XRF method described above to determine the geochemical composition of the dust. The fraction of dust composing the soil material was estimated using the following (Ferrier et al., 2011):

$$f_d = \left(\frac{Ti_r}{Ti_s} - \frac{Zr}{Zr_s}\right)\left[\frac{Ti_r - Ti_d}{Ti_s} - \frac{Zr_r - Zr_d}{Zr_s}\right]^{-1} \quad (2)$$

where Ti_r is the concentration of Ti in the rock, Ti_s is the concentration of Ti in the soil, Ti_d is the concentration of Ti in the dust, Zi_r is the concentration of Zr in the rock, Zr_s is the concentration of Zr in the soil, and Zr_d is the concentration of Zr in the dust. The resulting Ti/Zr ratios of the samples were also used to explore the geochemical characteristics at each field site.

Soils were pre-treated prior to quantitative x-ray diffraction to remove organic matter using NaOCl adjusted to pH 9.5 (Soil Survey Staff, 2009). The soils were ground to < 355 μm using a mortar and pestle. A known amount of zincite was added to the ground soil as an internal standard and micronized into a homogenous, bulk powder (< 180 μm) using a McCrone Micronizing Mill (Moore and Reynolds, 1997; Eberl, 2003) for quantitative x-ray diffraction. Rocks were broken using a mallet, or a sledgehammer when necessary, and internal, un-weathered fragments were selected from the specimen centers. Rock fragments were ground and processed using the preparation methods described for soils. Secondary mineral assemblage was determined using semi-quantitative x-ray diffraction (XRD). Briefly, oriented clay mounts were prepared on glass slides using the vacuum filtration method (Moore and Reynolds, 1997) with the standard suite of clay treatments including KCl-saturation, heat-treated KCl (300 °C and 550 °C), Mg-saturation, and Mg/glycerol solvation (Whittig and Allardice, 1986). Additionally, an aerosol formamide treatment was used to distinguish halloysite from kaolinite on Mg saturated samples (Churchman et al., 1984).

Oriented clay mounts and randomly oriented, bulk soil and rock powder mounts were analyzed by x-ray diffraction at the University of Arizona's Center for Environmental Physics and Mineralogy with a PANalytical X'Pert PRO Multi-Purpose Diffractometer (PANalytical, Almelo, The Netherlands). The system generated Cu-Kα x-rays at an accelerating potential of 45 kV, a current of 40 mA, and was equipped with a 1° divergence slit (1.52 mm), a 10 mm divergent mask, a 1° anti-scatter slit (1.52 mm), a 0.60 mm fixed receiving slit, and a sealed xenon detector fitted with a graphite monochromator. A spinner sample stage with a 1 s rotation time was used to measure from 4 to 65° 2-theta, with a step size of 0.020° and a dwell time of 3 s. Semi-quantitative x-ray diffraction was employed to determine secondary mineral assemblage where a fixed sample stage was used to measure oriented clay mounts with a scan range of 2–35° 2-theta, a step size of 0.040° and a dwell time of 3 s.

Quantitative phase analysis of the bulk soil and rock samples was completed using the full-pattern fit Rietveld refinement method (Bish and Post, 1993; Bish, 1994), an extension of the Rietveld method (Rietveld, 1969). The Rietveld method uses a least squares minimization process that relies on a set of user-defined crystal structure refinements to minimize differences between the observed diffraction pattern and the reference mineral patterns. The Rietveld refinements were performed in PANalytical X'Pert HighScorePlus v2.1b using reference mineral patterns from the RockJock Library and the American Mineralogist Crystal Structure Database (Downs and Hall-Wallace, 2003). The parameters selected for the refinement strategy sequence were based on Young's (1993) suggested parameter sequence. A set of global parameters, including R expected, weighted R, and goodness of fit generated by the software, were used to evaluate each refinement to ensure the production of accurate, high quality data (Speakman, 2013). Mineral phase quantification was independently confirmed by analyzing a subset of the rock and soil samples in RockJock (Eberl, 2003).

The resulting weight percentages for each mineral were averaged using all soils collected by each landscape position type in a given ecosystem (e.g., Table 2). The reported averages included 8 soil samples from two divergent pedons and 13 soils for two convergent pedons in the mixed conifer ecosystem. The respective number of soils used in the mineral percent averages for the desert system encompassed 6 samples from the two divergent positions and 8 samples from the 2 convergent positions. X'Pert HighScore Plus was utilized to estimate a biotite weight percent for dust using semi-quantitative x-ray diffraction instead of quantitative x-ray diffraction given sample size limitations for the dust materials. Characteristic secondary minerals were identified using HighScorePlus with reference mineral patterns from the RockJock Library and the American Mineralogist Crystal Structure Database.

3. Results

3.1. Quantitative mineralogy and mineral depth profiles

The primary mineral assemblage for the desert scrub and mixed conifer soils comprised ~30% quartz, whereas feldspar and micaceous minerals differed in abundance and type between ecosystems (Table 2). Primary mineral species in the desert soils included quartz, oligoclase,

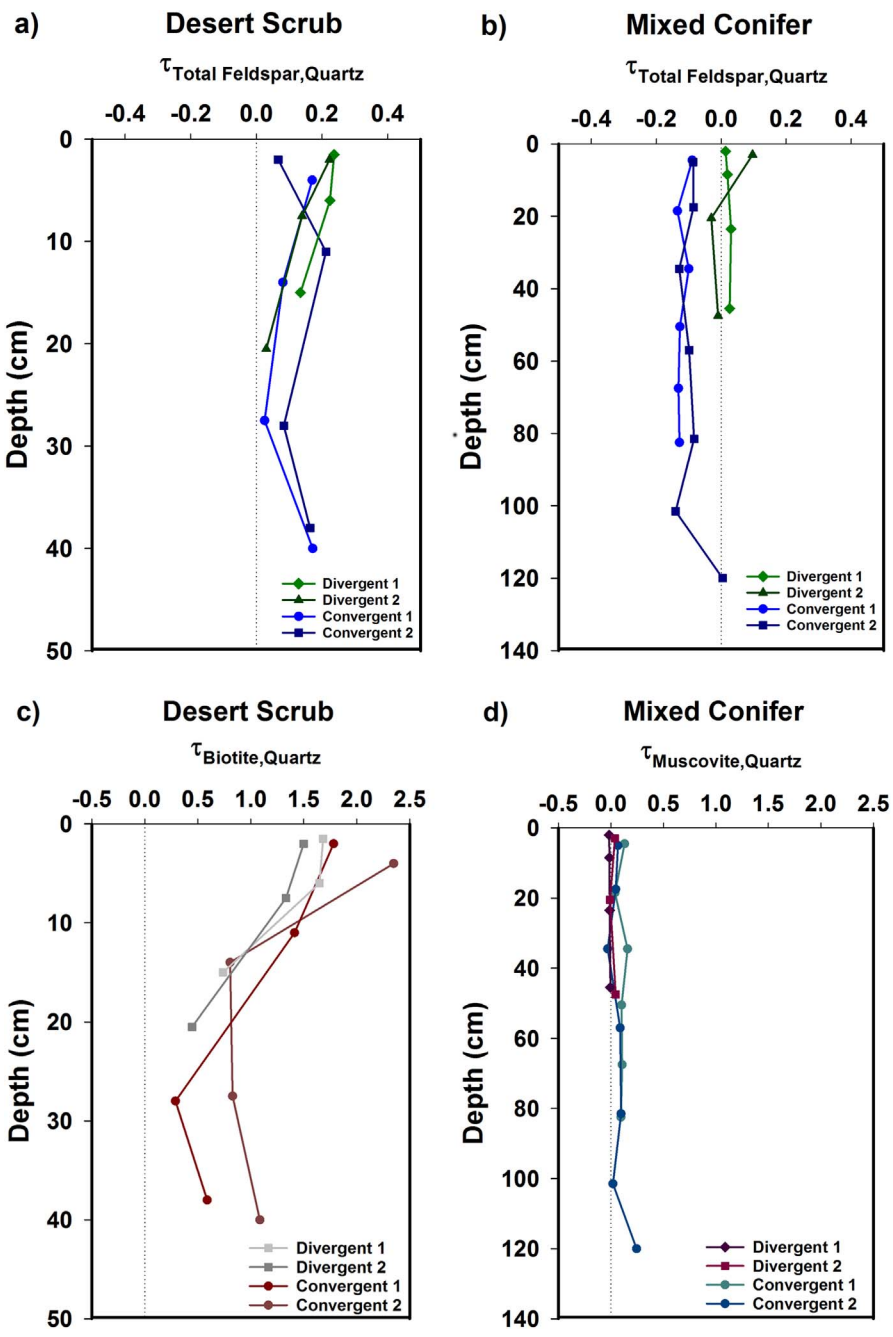

Fig. 2. Tau values for mineral constituents plotted by depth that include a) total feldspar in the desert scrub soils, b) total feldspar in the mixed conifer soils, c) biotite in the desert scrub soils, and d) muscovite in the mixed conifer soils.

orthoclase, and biotite compared to quartz, oligoclase, microcline, and both biotite and muscovite for soils in the mixed conifer system (Table 2; Fig. A3; Fig. A4). Biotite and muscovite co-occurred in the mixed conifer soils where the parent rock is comprised of two-mica granite (Table 1), with relative biotite abundances up to 1.4% compared with muscovite contents of 8 to 19%. All mixed conifer soil and rock powder diffractograms contained the 060 peak near 0.16 nm that indicates the presence of biotite or trioctahedral mica (Fig. A5). We observed no variation in mineral weight percentages by landscape position in the desert soils and minimal change in the mixed conifer soils.

Mineral tau depth profiles for the desert soils revealed additions of feldspar (Fig. 2a; Fig. A1a; Fig. A2a) and biotite (Fig. 2c) relative to quartz. Tau values for total feldspar indicated enrichment in the profile, with gains of 3 to 24% and 2 to 22% in divergent and convergent soils, respectively (Fig. 2a). Substantial biotite enrichment was recognized for both landscape positions with the divergent sites exhibiting gains of 45 to 168% and 29 to 235% in convergent positions (Fig. 2c). Surface soils showed the greatest degree of biotite enrichment in both positions.

The mixed conifer soils presented hillslope scale differences in tau depth profiles for total feldspar (Fig. 2b; Fig. A1b; Fig. A2b) and muscovite (Fig. 2d). Convergent sites demonstrated relatively consistent depletions of total feldspar in both pedons, except for the saprock, which exhibited little change from the parent material (Fig. 2b). The divergent sites showed slight enrichment of total feldspar in the surface soils and little change from the parent rock with depth. The convergent positions were also slightly enriched in muscovite with a maximum enrichment of 24% in the saprock while one subsurface horizon did exhibit a loss of 3%. Muscovite was slightly enriched throughout both divergent pedons with gains ranging from a maximum of ~20% in the surface soils to 3–5% in the subsurface (Fig. 2d).

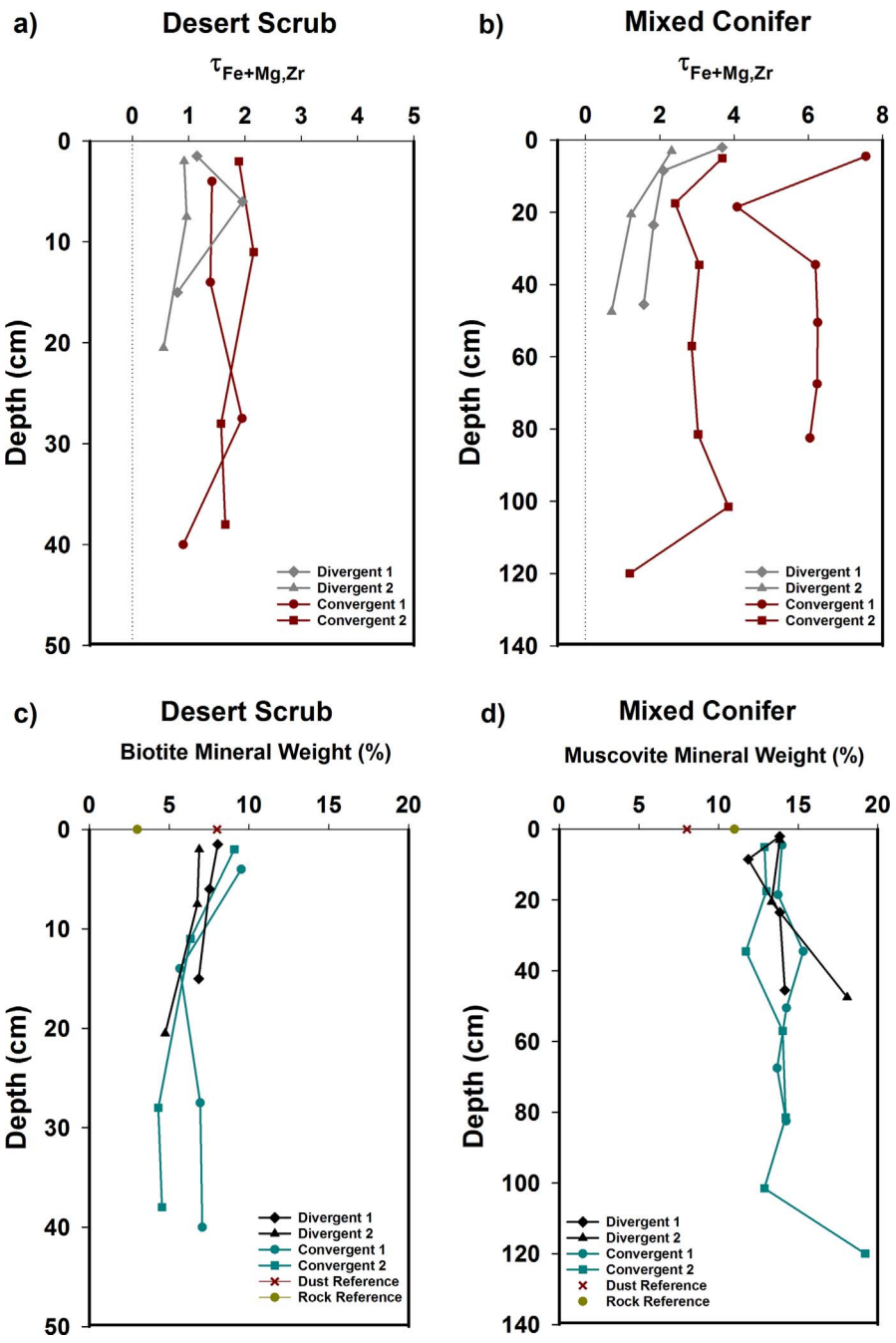

Fig. 3. Desert scrub geochemical and mineralogical data including a) Fe + Mg tau values versus depth in the desert scrub soils, b) Fe + Mg tau values versus depth in the mixed conifer soils, c) biotite mineral weight percent as a function of depth in the desert scrub soils, and d) muscovite mineral weight percent as a function of depth in the mixed conifer soils.

3.2. Elemental and mineralogical profiles for desert and mixed conifer soils

Desert scrub soils were enriched in Fe + Mg with gains of 90 to 215% for convergent profiles, and 55 to 196% for divergent profiles (Fig. 3a). Corresponding depth plots for biotite weight percent indicates that surface soils contain the highest concentrations of biotite that decrease with depth in both landscape positions (Fig. 3b). Biotite percentages in surface soils also coincide well with an estimated mineral weight percent of ~8% for biotite in reference dust material from the desert scrub site (Fig. 3c).

The mixed conifer sites exhibited substantial enrichment in Fe + Mg, with gains of ~300% in surface soils of the divergent profiles and ~70% in the subsurface. We observed gains of 750% to ~95% for convergent profiles (Fig. 3b). Muscovite weight percentages in the divergent soils ranged from 12% in the near-surface soils to 18% in the saprock compared to 12 to 19% in convergent sites. (Fig. 3d). The mineral weight percentages for muscovite in the soils closely align with those for rock reference material (Fig. 3d) as do the tau values that show near zero change in muscovite relative to the parent rock (Fig. 2d).

Losses of Na, Si, and K + Ca occurred in both the desert and mixed conifer soil profiles. Depletion profiles for the desert soils showed no differences between landscape positions, with the overarching trend indicating greater elemental loss in surface soils (Fig. 4a–c). Conversely, the mixed conifer sites exhibited distinct patterns of depletion by landscape position for Na (Fig. 4d), Si (Fig. 4e), and K + Ca (Fig. 4f), with the greatest degree of loss in the convergent profiles.

3.3. Dust fraction estimates and elemental ratios

The accumulation of biotite, Fe + Mg, and total feldspars in the surface soils of both sites led to a geochemical examination of dust in

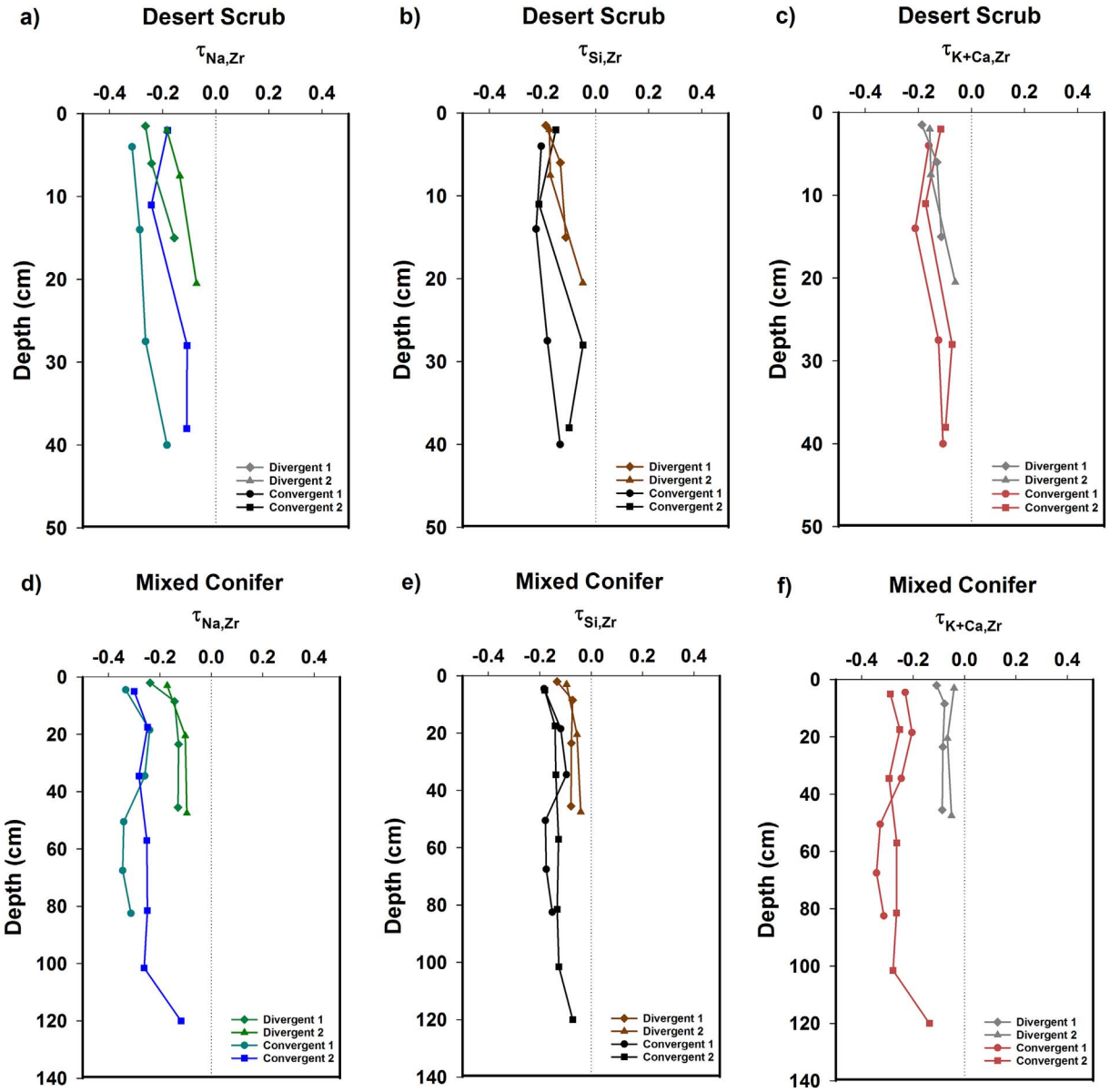

Fig. 4. Geochemical depth profiles for the desert scrub site including a) $\tau_{Na,Zr}$, b) $\tau_{Si,Zr}$, c) $\tau_{K\ +\ Ca,Zr}$. Geochemical depth profiles for the mixed conifer site that include d) $\tau_{Na,Zr}$, e) $\tau_{Si,Zr}$, and f) $\tau_{K\ +\ Ca,Zr}$.

the soil profiles. Dust fraction estimates for the desert scrub system ranged from 2 to 16% in the divergent positions and 6 to 21% in the convergent landscapes. Dust fraction inputs to the mixed conifer landscapes ranged from 13 to 19% in the divergent sites and 9 to 19% in the convergent positions (Table 3).

3.4. Secondary mineral assemblage

Clay mineral assemblages were comprised of 1:1 and 2:1 phyllosilicates that varied in composition with depth, landscape position, and ecosystem. Clay minerals in the desert soils included vermiculite, smectite, hydrated halloysite, dehydrated halloysite and/or kaolinite, and interlayered halloysite/kaolinite-smectite. The smectite minerals were present in all desert scrub soils with expansion of 1.0 nm peaks to 1.8 nm following Mg saturation/glycerol solvation (Fig. 5a; Fig. 6a). The surface horizons of both desert landscape positions contained hydrated or partially dehydrated halloysite, with peaks at 1.0 nm, accompanied by broadly shaped peaks at 0.7 nm that expanded towards 1.0 nm with formamide solvation, suggesting a dehydrated halloysite (Churchman et al., 1984; Churchman, 1990) (Figs. 5a, 6a). Confirming the presence or absence of 1.0 nm halloysite in the convergent location was challenging due to the presence of a 1.0 nm illite peak that does not expand with Mg saturation and glycerol solvation. However, the lack of crystallinity of the 1.0 nm peak in the Mg-glycerol treatment suggests the presence of 1.0 nm halloysite rather than illite. The hydrated halloysite peaks decreased in intensity with depth while the 0.7 nm peaks remained similar throughout the profiles. Minor amounts of vermiculite were also detected at 1.4 nm in the desert scrub horizons.

Soils in the divergent positions of the desert scrub ecosystem contained interlayered halloysite/kaolinite-smectite minerals that were distinguished by 1) the partial collapse of the species during K^+ saturation and K^+-550 heat treatments and 2) the presence of a peak in the 0.750–0.755 nm range that exhibited minimal collapse after K-saturation and K-300 heat treatments (Fig. 5a; Corti et al., 1998). We did not observe these patterns in the adjacent convergent positions where full collapse during heat treatment occurred (Fig. 6a).

Clay mineral assemblage of the mixed conifer soils were dominated by vermiculite, hydroxy-interlayed vermiculite (HIV), illite, and kaolin

Table 3
Dust fraction estimates (f_a) determined for each soil horizon using the Ferrier et al. (2011) method.

Pedon	Top depth (cm)	Bottom depth (cm)	Dust fraction estimate (f_a)
Mixed conifer			
Divergent 1	0	4	0.13
	4	13	0.13
	13	34	0.15
	34	57	0.14
Divergent 2	0	6	0.19
	6	35	0.14
	35	60	0.13
Convergent 1	0	9	0.19
	9	28	0.12
	28	41	0.12
	41	60	0.13
	60	75	0.18
	75	90	0.16
Convergent 2	0	10	0.10
	10	25	0.10
	25	44	0.09
	44	70	0.10
	70	93	0.13
	93	110	0.13
	110	130	0.15
Desert scrub			
Divergent 1	0	3	0.08
	3	9	0.16
	9	21	0.13
Divergent 2	0	4	0.02
	4	11	0.02
	11	30	0.00
Convergent 1	0	8	0.08
	8	20	0.10
	20	35	0.16
	35	45	0.06
Convergent 2	0	4	0.16
	4	18	0.15
	18	38	0.16
	38	38	0.21

peaks (Fig. 5b, Fig. 6b). The conifer divergent saprock contained a small gibbsite peak (Fig. 5b) and minor smectite peaks were present in convergent and divergent saprock. The sharp 1.0 nm illite peak in the surface conifer soils decreased in intensity with depth, particularly in the divergent site.

4. Discussion

4.1. Climate and topographic controls on element and mineral distribution

Climate and topography represent interactive controls on the weathering of silicate minerals as evidenced by the greatest depletion of total feldspars in the water-gathering convergent positions of the mixed conifer site (Fig. 2b). The data indicated a greater degree of mineral transformation, elemental loss, and desilication in the wetter, more biologically productive conifer ecosystems (Figs. 2, 4), which aligned with findings from other climate gradient studies (Dahlgren et al., 1997; Oh and Richter, 2005; Graham and O'Geen, 2010; Yousefifard et al., 2012; Khomo et al., 2013).

Element and mineral losses in the mixed conifer ecosystem were greatest in the convergent landscapes, demonstrating an increase in downslope mineral weathering similar to prior *catena* studies (Nettleton et al., 1968; Hattar et al., 2010; Khomo et al., 2011). The influence of topography was less evident in the desert system, likely a result of drier site conditions and the added complexity of dust inputs to the shallow desert soils. We predict that the additions of feldspar (Fig. 2a) and biotite (Fig. 3a) to the desert system originate from dust inputs that alter the geochemical composition of the soils and complicate the assessment of *in situ* weathering.

4.2. Dust fraction estimates in the SCM

Our findings indicate that dust comprises up to ~20% of the soil material in the SCM desert and conifer ecosystems (Table 3), which has important implications for soil geochemistry and nutrient cycling. The dust fraction ranges for the SCM align with estimates of 10 to 40% in the San Juan Mountains, Colorado (Lawrence et al., 2011) and 5 to 45% for soils on cinder cones in northern Arizona (Rasmussen et al., 2017), but were lower than the 50 to 100% reported for soils in drier regions (Crouvi et al., 2013; McFadden, 2013). Dust-derived enrichments in silt are common in low and high elevation landscapes (Wells et al., 1985; Dahms, 1993; Bockheim and Koerner, 1997; Muhs and Benedict, 2006). We see evidence for this phenomenon in the mixed conifer field sites, with higher end member dust estimates corresponding to greater average pedon silt contents (Table 3; Lybrand and Rasmussen, 2015). The higher dust estimates for the mixed conifer site may reflect more dust trapped by densely vegetated forests, where the rough, extensive surfaces of trees intercept dust inputs, including dust-derived nutrients, in a process known as canopy trapping (e.g., Lawrence et al., 2011).

4.2.1. Dust-derived minerals as a source of nutrients

The dust-derived minerals in the SCM soils may represent a potential source of nutrients to the desert and conifer ecosystems. The gains of total feldspar in the desert soils coincide with elemental depletions of Na, Si, and Ca + K (Fig. 4a–c), suggesting that the minerals in the dust underwent transformation either in situ or prior to deposition. Backscattered electron images of dust collected from the desert site indicated that the dust did contain fine-grained weathered minerals (Fig. 7a–d). We expect that these smaller transformed grains prove more accessible to organisms compared to larger, resistant grains that originate from the granite bedrock. The dust may also be provide elements that are inherently low in granite parent material, such as P. Aciego et al. (2017) identified dust as a critical contributor of P to the nutrient budget for the montane forests in the Sierra Nevada, with P concentrations in the dust being 2.5 times greater than P in the actively eroding granitic bedrock. We also observed that P concentrations were 2 to 3 times higher in dust and surface soil samples from our sites when compared to abundances in parent rock (Lybrand, 2014). The elemental and mineralogical constituents of dust signify a valuable source of nutrients to ecosystems that requires further examination, especially in forested landscapes where dust inputs are underrepresented.

4.2.2. Elemental enrichments of Fe and Mg from deposition of dust

The desert scrub and mixed conifer soils exhibited unanticipated gains in Fe and Mg (Fig. 3a,b) that we associate with dust-derived minerals including biotite. Biotite grains occur in dust (Fig. 7a–d) and biotite percentages in the desert soils were more than double those measured in the parent rock (Fig. 3c). The desert soils showed gains in Fe and Mg corresponding to biotite mineral weight percentages that closely matched semi-quantitative estimates of biotite in dust samples (Fig. 3a,c). Enrichments in Fe and Mg occurred throughout all four profiles in the mixed conifer site with the greatest additions in the surface soils (Fig. 3b), which suggest external inputs and/or biocycling.

We predict that the lower abundance of biotite in the mixed conifer soils results from the transformation of dust-derived biotite grains to secondary weathering products, such as illite and vermiculite (Fig. 5b; Fig. 6b). Both illite and vermiculite contain the Fe and Mg that would contribute to the enrichment of these elements despite low percentages of biotite in the conifer ecosystem.

Elemental additions of Fe and Mg in both the desert and conifer ecosystems were most pronounced in convergent positions, particularly in the conifer system (Fig. 3b). We attribute these gains to dust inputs to the soil surface that were subsequently redistributed by erosion (Brantley et al., 2007). Our results support the notion that topography acts a hillslope-scale control on the redistribution and accumulation of dust following deposition (Crouvi et al., 2013).

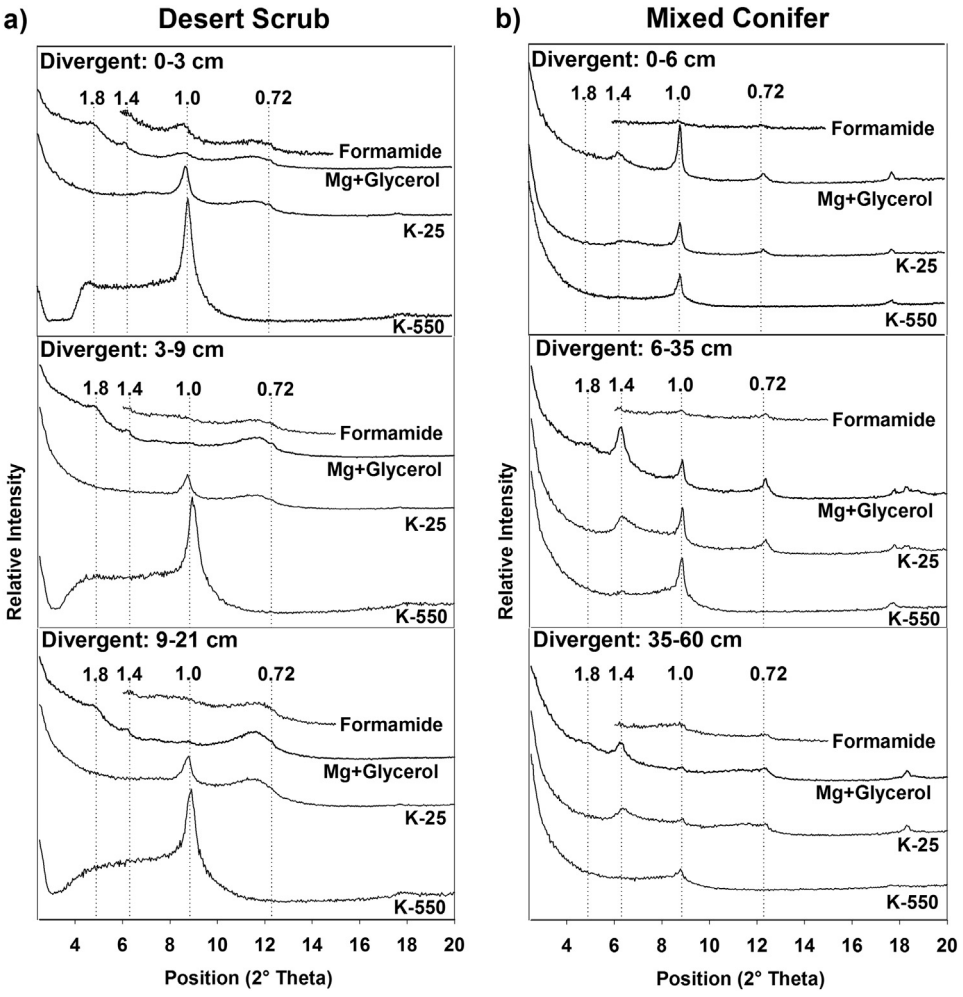

Fig. 5. X-ray diffractograms of clay fractions for Mg + Glycerol, formamide, K-25, and K-550 treatments in the divergent landscape positions for the a) desert scrub and b) mixed conifer sites.

Enrichments of Fe and Mg correspond to dust inputs in other granitic landscapes where proximity to dust sources was a key factor (Dixon et al., 2012; Khomo et al., 2013). A study of chemical weathering in the San Gabriel Mountains, California found soils on the eastern side of the mountain range to be enriched in Fe and Mg compared to western sites (Dixon et al., 2012). The authors postulated that the eastern sites received higher dust inputs from the Mojave Desert than the more distant western landscapes (Dixon et al., 2012). Mojave dust contains notable concentrations of Fe and Mg (Reheis and Kihl, 1995) and likely had an impact on the geochemistry of the nearby (< 20 km) soils examined by Dixon et al. (2012).

We speculate that dust deposition occurs throughout the SCM given the array of regional to local scale dust sources in southern Arizona (Clements et al., 2013) and the documented impacts of dust on high elevation sites in the western United States (Muhs and Benedict, 2006). Dust sources in the southwest include alluvial deposits, playas, barren agriculture land, post-fire disturbances, and wind-driven disturbance during monsoon events (Clements et al., 2013; Hahnenberg and Nicoll, 2014), all of which may contribute to the dust measured in the SCM.

Substantial Fe and Mg enrichments have been identified in lower hillslope positions compared to upslope landscapes (Khomo et al., 2013). Significant gains in Fe and Mg were observed in a study of arid *catena* soils where granitic soils located closest to a basalt dust source exhibited substantial enrichment in these elements compared to soils located further away (> 15 km) (Khomo et al., 2013). The greater gains in Fe and Mg in the downslope landscape position is similar to the SCM soils where the greatest enrichments occurred in the convergent positions, likely reflecting contributions from local and upslope dust deposits. The dust fraction of soil in a downslope landscape position is a product of local dust inputs to that given geomorphic position, as well as contributions from upslope soils that were transported downslope (Crouvi et al., 2013).

4.3. Secondary mineral assemblage across the environmental gradient

4.3.1. Desert soils

The degree of mineral alteration intensified in the cool, wet conifer soils compared to the desert system, leading to distinct differences in secondary mineral assemblages. The desert clay minerals included vermiculite, smectite, hydrated/partially dehydrated halloysite/kaolinite, and interlayered halloysite/kaolinite-smectite (Fig. 5a; Fig. 6a). We predict that the partial collapse of the halloysite/kaolinite-smectite minerals in the divergent position compared to full collapse in the convergent sites reflects a greater degree of mineral transformation in the wetter, downslope positions. The dominant minerals, smectite and halloysite, suggest a weathering-limited, silica-rich environment (Parfitt et al., 1983; Dahlgren et al., 1997; Ziegler et al., 2003; Graham and O'Geen, 2010). Smectites form through inheritance from parent materials, 2:1 phyllosilicate mineral transformations, or neoformation where smectites precipitate from soil solutions (Reid-Soukup and Ulery, 2002). Neoformed smectites precipitate under basic soil conditions where silica and magnesium concentrations are high (Jackson, 1965; Weaver et al., 1971). We expect that the smectites identified in the desert scrub soils were neoformed given conducive soil conditions, yet the transformation of biotite is also possible.

Halloysite was an unexpected mineral identified in the desert scrub

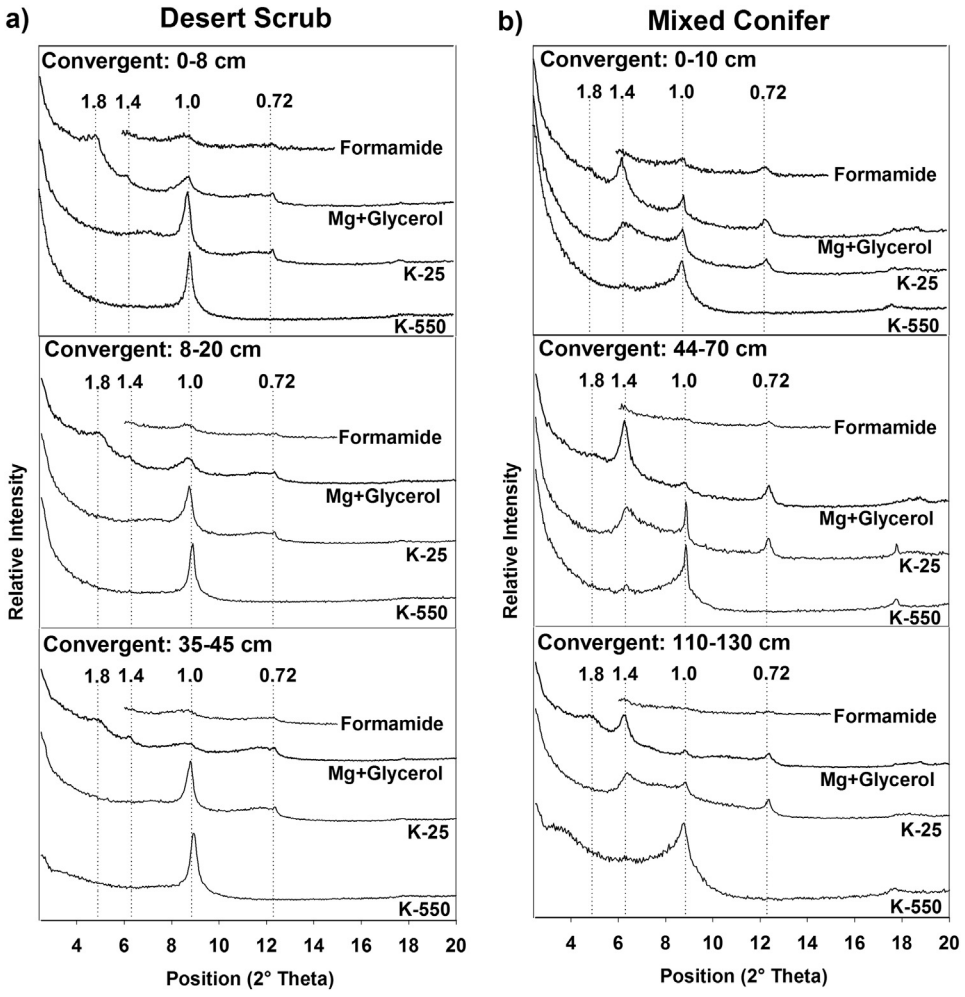

Fig. 6. X-ray diffractograms of clay fractions for Mg + Glycerol, formamide, K-25, and K-550 treatments in the convergent landscape positions for the a) desert scrub and b) mixed conifer sites.

soils (Fig. 5a; Fig. 6a). Halloysite has been identified under different conditions ranging from humid, tropical climates (Gilkes et al., 1980; Jeong et al., 2003), to volcanic ash soils (Parfitt et al., 1983; Rasmussen et al., 2007), to weathered granitic terrain (Robertson and Eggleton, 1991; Taboada and Garcia, 1999), to drier environments where minimal leaching concentrated silica in soils (Parfitt et al., 1983). Halloysite was also documented as a metastable product of basalt weathering in arid soils of Hawai'i (Ziegler et al., 2003) via kinetic factors, where rapid wet/dry cycles inhibited the thermodynamically predicted formation of smectite.

Interestingly, smectite and halloysite co-occur in the desert soils, which we attribute to microscale differences in solution chemistry or mineral texture that promotes the precipitation of both mineral phases. Halloysite and kaolinite minerals also differ in chemical and morphological compositions, and co-exist in soil profiles (Churchman and Gilkes, 1989; Banfield and Eggleton, 1990; Papoulis et al., 2004); an observation associated with microtexture controls and the composition of soil solution (Papoulis et al., 2004). For example, halloysite and kaolinite co-occurred in granitic saprolite where halloysite formed in the microfissures of transforming plagioclase and kaolinite from weathered biotite (Jeong, 2000), supporting the potential for localized clay precipitation in contrasting microenvironments. We attribute the complex array of smectite, hydrated and dehydrated halloysite/kaolinite, and interlayered halloysite/kaolinite-smectite to climatic, soil, and mineral microtextural interactions in the dry desert environment.

The distribution of kaolin mineral phases also changed with soil depth in the desert scrub soils (Fig. 6a), likely a function of moisture availability and rapid periods of wetting and drying. An increase in hydrated halloysite with depth is common in xeric soil moisture regimes where prolonged drying cycles in the summer months may dehydrate halloysite in the surface soils (Takahashi et al., 1993). A transition from kaolinite to dehydrated halloysite was identified when comparing surface to subsurface soils in lateritic weathering profiles (Churchman and Gilkes, 1989) and in a study of volcanic soil development across sites with xeric soil moisture regimes in California (Rasmussen et al., 2010). Surprisingly, the desert scrub surface soils in both landscape positions exhibited the strongest hydrated halloysite peaks that decreased in intensity and transitioned to dehydrated halloysite and/or kaolinite with depth (Fig. 6a). Episodic, intense monsoons may provide the moisture required for the halloysite to remain hydrated in the shallow surface soils (< 10 cm) during the summer months.

4.3.2. Mixed conifer soils

The mixed conifer soils exhibited the greatest degree of mineral transformation in the SCM where clay minerals included vermiculite, illite, kaolinite, and HIV, with smectite and gibbsite as minor constituents. Greater moisture availability at the conifer sites corresponded to more intense kaolinite peaks with respect to smectite, a trend suggesting increased desilication. Vermiculite was identified in both divergent and convergent landscape positions (Fig. 5b, Fig. 6b). Vermiculite is widely distributed in soils and is a common intermediate weathering product resulting from the transformation of biotite and muscovite (Malla, 2002). We observed a sharp 1.0 nm illite peak that decreased in intensity with depth coupled with little to no smectite in the divergent landscape positions (Fig. 5b), yet smectite and evidence

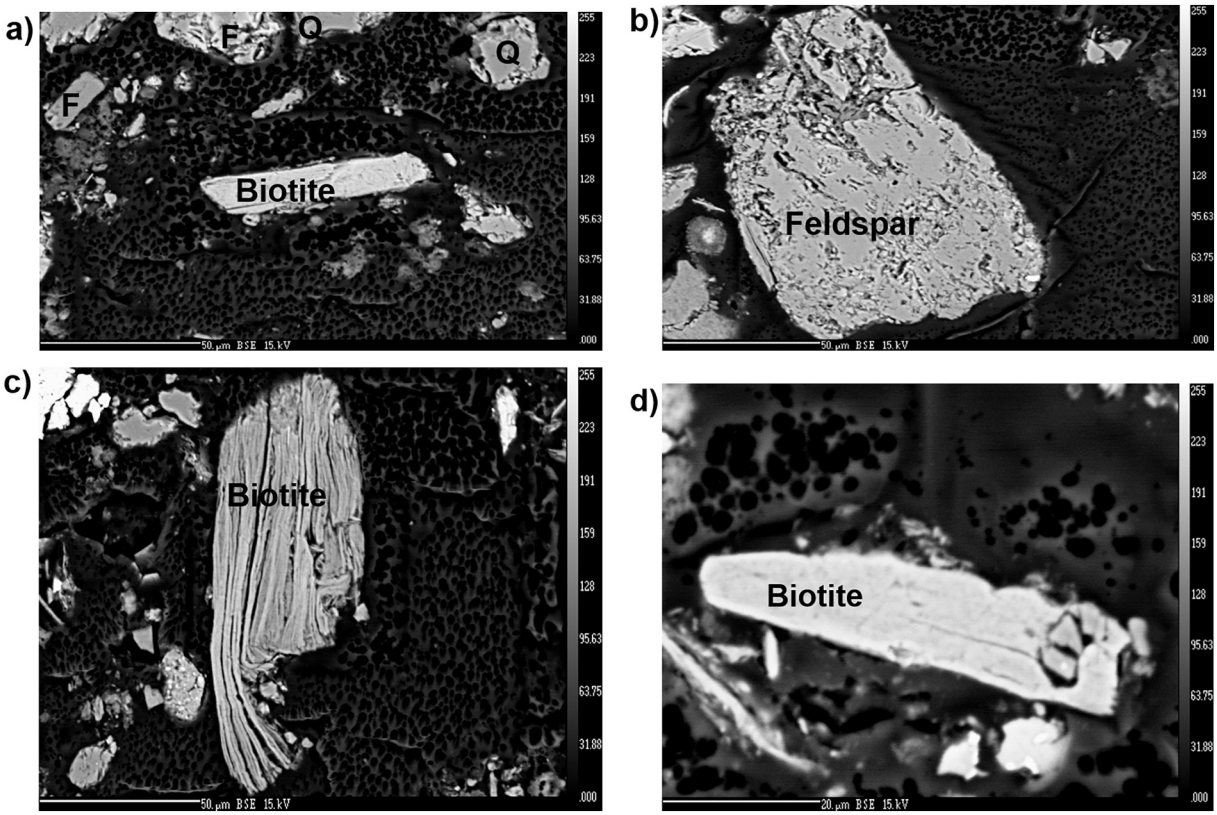

Fig. 7. Backscattered electron images of transformed grains in dust samples collected at the desert scrub site. In the images, F denotes feldspar and Q signifies quartz.

for the presence of interstratified minerals was observed in the convergent soils, particularly the shallow saprock at ~40 cm (Fig. 6b). We attributed the sharp illite peaks in the divergent positions to dust inputs that became less prevalent with depth whereas the occurrence of smectite and interstratified minerals in the saprock may result from the accumulation of soluble weathering products (e.g., Si) in the convergent water-gathering position. Well-expressed smectite peaks were also noted at the soil- rock interface in a dry oak woodland site in California where solutes likely accumulated and precipitated smectite due to contact with a consolidated parent rock horizon (Rasmussen et al., 2010). Smectite formation has been detected in lower footslope positions with marked absences in adjacent crest and near-crest positions (Khomo et al., 2011), an observation attributed to greater concentrations of water-soluble Mg and Si transported downslope (Graham and O'Geen, 2010).

Hydroxy-interlayered vermiculite is a common mineral phase resulting from muscovite weathering where vermiculite is interlayered with Al (Malla, 2002). The formation of the hydroxyl-Al interlayered vermiculite often results in an "anti-gibbsite effect," where Al concentrations are lowered in soil solution thereby discouraging gibbsite precipitation (Jackson, 1963). Surprisingly, HIV and gibbsite co-occurred in the divergent saprock that we associate with differences in microscale environments (Bhattacharyya et al., 2000).

The gibbsite identified in the mixed conifer divergent saprock was unexpected, particularly in a climatic regime receiving < 140 cm of precipitation a year (Vazquez, 1981), and could result from localized primary mineral transformations. Gibbsite formation has been categorized as "primary gibbsite" and "secondary gibbsite" where "primary gibbsite" originates from the initial stages of aluminosilicate weathering of parent rock minerals and "secondary gibbsite" from long-term kaolinite weathering reactions (Boulange et al., 1975). Gibbsite has been documented in young, non-tropical environments (Wada and Aomine, 1966; Reynolds, 1971; Vazquez, 1981) and has been found crystallized on plagioclase mineral surfaces during the initial stages of transformation (Tazaki, 1976). The conditions outlined for "primary gibbsite" formation include well-drained soil environments subjected to rapid water flow that removes base cations and silica from the weathering system (Vazquez, 1981). "Primary gibbsite" is most common on hillslopes and is found less frequently in depositional valleys, likely a result of the redistribution of water and weathering constituents across a *catena*. Furthermore, "primary gibbsite" is most abundant in C mineral horizons due to its origin in the weathered parent rock (Vazquez, 1981). We propose that the minor amount of gibbsite detected in our study originated from the initial stages of granitic saprock weathering in the well-drained divergent landscape positions. Prior work on the conifer divergent saprock confirmed microscale depletions of Na and Si across plagioclase grains and in-situ clay weathering products (Lybrand and Rasmussen, 2014), evidence for a low-silica environment that may be conducive to gibbsite precipitation.

5. Summary

The geochemical and mineralogical properties of granitic soils were examined by landscape position across an environmental gradient in southern Arizona. Mineral and base cation losses were highest in convergent positions, with greater relative loss in the wetter conifer ecosystems. Clay mineral assemblage in the warm, dry desert soils was dominated by halloysite and smectite, reflecting climatic and mineral microtextural controls on secondary phase formation. Clay minerals in the conifer soils exhibited a greater degree of transformation, consisting of vermiculite, illite, kaolinite, and minor amounts of smectite and gibbsite. Enrichments in minerals (e.g., total feldspar, biotite) and select elements (e.g., Fe, Mg) suggest that dust contributed to the mineral and/or elemental composition of soils in all sites, with dust fraction estimates up to ~20% in the desert scrub and mixed conifer soils.

Our findings indicate that climate, topography, and dust serve as interactive controls on mineral composition and soil geochemistry in the Catalina Critical Zone Observatory. We expect that the fine-grained,

transformed minerals deposited as dust represent a source of nutrients to ecosystems in the Sky Island region, particularly in the desert environments where rock-derived minerals have undergone little to no in situ transformation. The role of dust-derived minerals and associated nutrients must be addressed when examining soil and critical zone development in the southwestern U.S.

Acknowledgements

This research was funded by the University of Arizona Agricultural Experiment Station ARZT-1367190-H21-155, NSF EAR-1123454, NSF EAR/IF-0929850, and the National Critical Zone Observatory program via NSF EAR-0724958 and NSF EAR-13331408. The authors also thank Jon Pelletier, Onn Crouvi, S. Mercer Meding, Katarena Matos, Molly van Dop, Justine Mayo, Stephanie Castro, Christopher Clingensmith, Mary Kay Amistadi, Stephan Hlohowskyj, and Andrew Martinez for laboratory and field assistance.

Appendix A

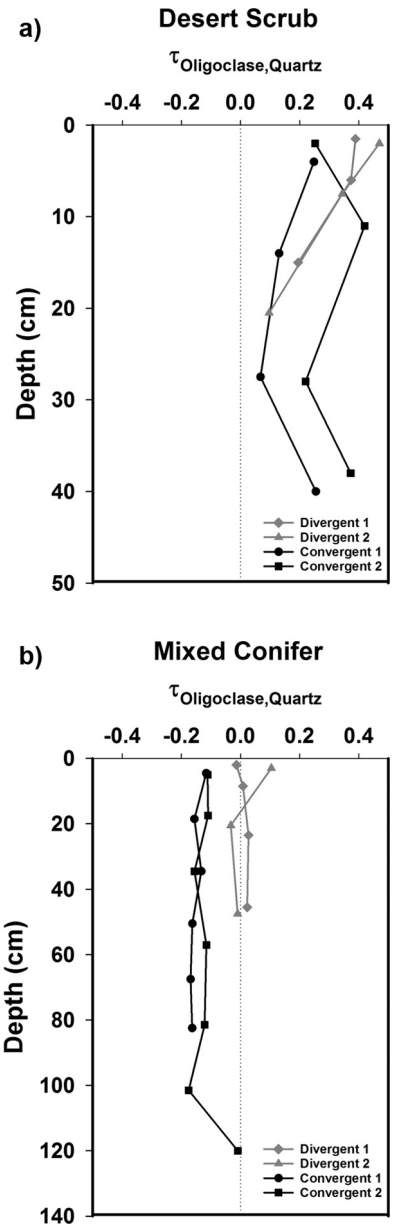

Fig. A1. Mobile constituent, oligoclase, in the a) desert scrub and b) mixed conifer sites.

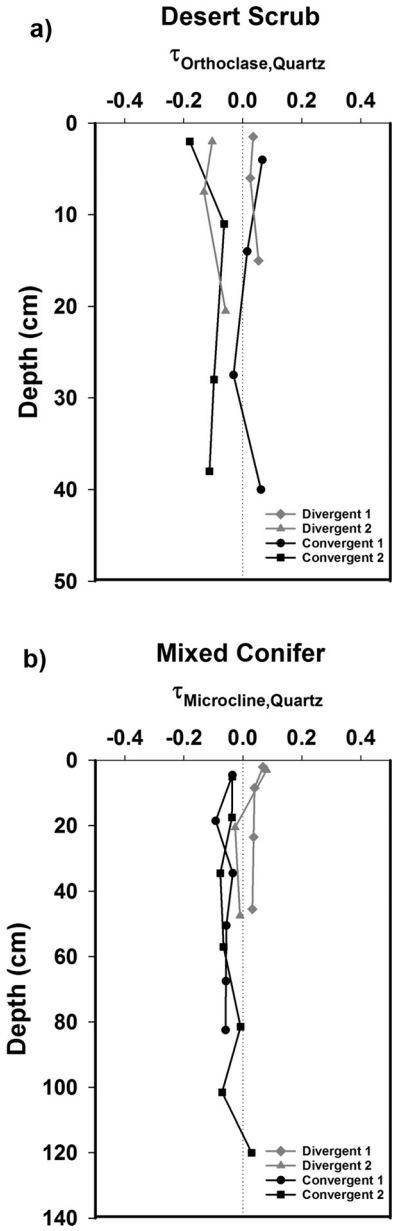

Fig. A2. Mobile potassium feldspar constituents including a) orthoclase in the desert scrub soils and b) microcline in the mixed conifer soils.

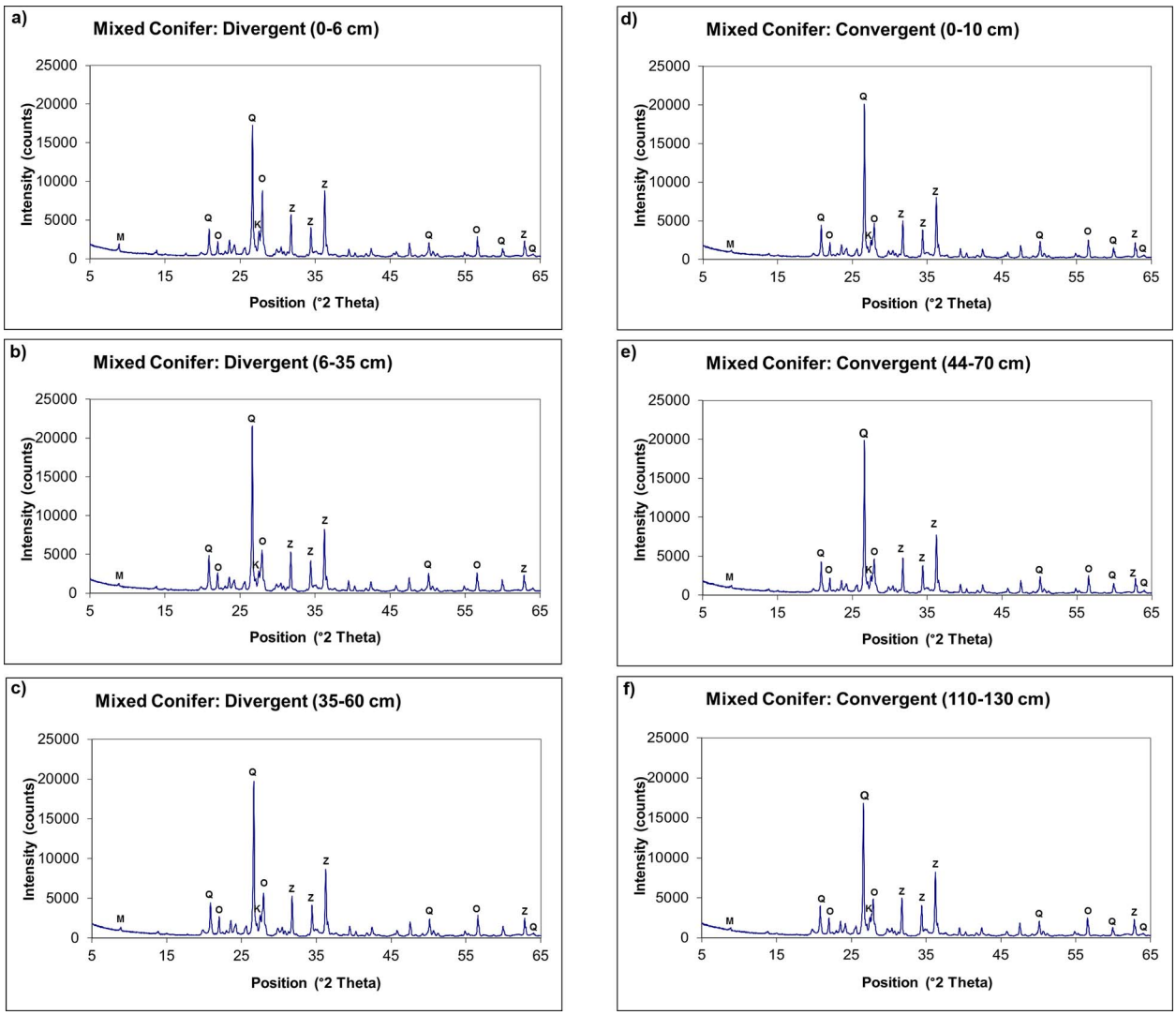

Fig. A3. X-ray diffraction patterns of soils from the mixed conifer site analyzed as bulk random powder mounts. A depth profile for the divergent position included soils examined at the following depths: a) 0–6 cm; b) 6–35 cm; and c) 35–60 cm. A depth profile for the convergent position spanned d) 0–10 cm; e) 44–70 cm; and f) 110–130 cm. Letter abbreviations in the figures include M = mica (muscovite/biotite for mixed conifer field area); Q = quartz; O = oligoclase; K = K-feldspar (microcline for mixed conifer field area); and Z = zincite (internal standard).

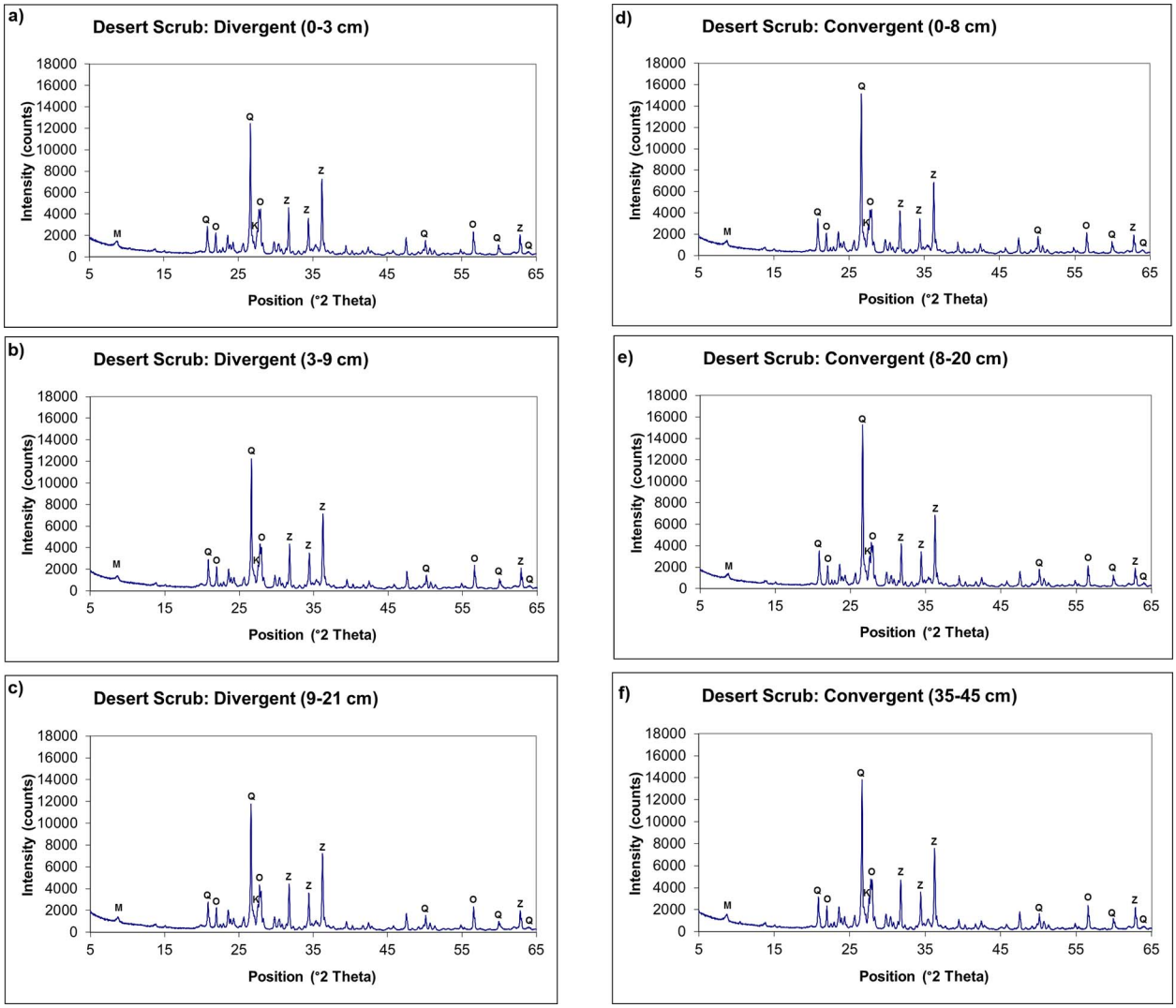

Fig. A4. X-ray diffraction patterns of soils from the desert scrub site analyzed as bulk random powder mounts. A depth profile for the divergent landscape position included soils examined at the following depths: a) 0–6 cm; b) 6–35 cm; and c) 35–60 cm. A depth profile for the convergent position spanned d) 0–10 cm; e) 44–70 cm; and f) 110–130 cm. Letter abbreviations in the figures include M = mica (biotite for desert field area); Q = quartz; O = oligoclase; K = K-feldspar (orthoclase for the desert field area); and Z = zincite (internal standard).

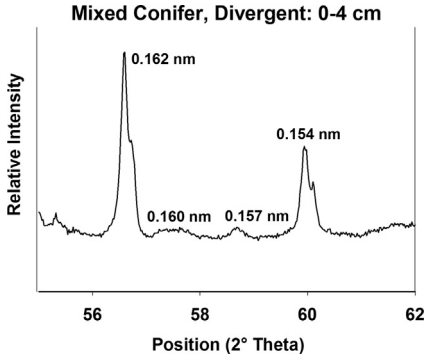

Fig. A5. Example of peaks in the 0.16 nm range that confirm the presence of biotite or trioctahedral mica.

References

Aciego, S.M., Riebe, C.S., Hart, S.C., Blakowski, M.A., Carey, C.J., Aarons, S.M., Dove, N.C., Botthoff, J.K., Swims, K.W.W., Aronson, E.L., 2017. Dust outpaces bedrock in nutrient supply to montane forest ecosystems. Nature 8, 14800.

Banfield, J.F., Eggleton, R.A., 1990. Analytical transmission electron microscope studies of plagioclase, muscovite, and K-feldspar weathering. Clay Clay Miner. 38, 77–89.

Barshad, I., 1966. The effect of the variation in precipitation on the nature of clay mineral formation in soils of acid and basic igneous rocks. In: Proceedings of the International Clay Conference. 1. Israel, Jerusalem, pp. 167–173.

Berner, R.A, Lasaga, A.C., Garrels, R.M., 1983. The carbonate-silicate geochemical cycle and its effect on atmospheric carbon dioxide over the past 100 million years. Am. J. Sci. 283, 641–683.

Berry, M.E., 1987. Morphological and chemical characteristics of soil catenas on Pinedale and Bull Lake moraine slopes in the Salmon River Mountains, Idaho. Quat. Res. 28, 210–225.

Bhattacharyya, T., Pal, D.K., Srivastava, P., 2000. Formation of gibbsite in the presence of 2:1 minerals: an example from Ultisols of northeast India. Clay Miner. 35, 827–840.

Birkeland, P.W., 1999. Soils and Geomorphology. Oxford University Press, New York.

Bish, D.L., 1994. Quantitative X-ray diffraction analysis of soils. In: Amonette, J.E., Zelazny, L.W. (Eds.), Quantitative Methods in Soil Mineralogy. Soil Science Society of America, Madison, USA, pp. 267–295.
Bish, D.L., Post, J.E., 1993. Quantitative mineralogical analysis using the Rietvetd full-pattern fitting method. Am. Mineral. 78, 932–940.
Bockheim, J.G., Koerner, D., 1997. Pedogensis in alpine ecosystems of the Eastern Uinta Mountains, Utah, U.S.A. Arct. Alp. Res. 29, 164–172.
Bockheim, J.G., Munroe, J.S., Douglass, D., Koerner, D., 2000. Soil development along an elevational gradient in the southeastern Uinta Mountains, Utah, USA. Catena 39, 169–185.
Boulange, B., Paquet, H., Bocquter, G., 1975. Le role de l'argile dans la migration et l'accumulation de l'alumine de certaines bauxites tropicales. C. R. Acad. Sci. 280D, 2183–2186.
Brantley, S.L., Goldhaber, M.B., Ragnarsdottir, K.V., 2007. Crossing disciplines and scales to understand the Critical Zone. Elements 3, 307–314.
Bullard, J.E., Harrison, S.P., Baddock, M.C., Drake, N., Gill, T.E., McTainsh, G., Sun, Y., 2011. Preferential dust sources: a geomorphological classification designed for use in global dust-cycle models. J. Geophys. Res. 116 (F04034).
Churchman, G.J., 1990. Relevance of different intercalation tests for distinguishing halloysite from kaolinite in soils. Clay Clay Miner. 38, 591–599.
Churchman, G.J., Gilkes, R.J., 1989. Recognition of intermediates in the possible transformation of halloysite to kaolinite in weathering profiles. Clay Miner. 24, 579–590.
Churchman, G.J., Whitton, J.S., Claridge, G.G.C., Theng, B.K.G., 1984. Intercalation method using formamide for differentiating halloysite from kaolinite. Clay Clay Miner. 32, 241–248.
Clements, A.L., Fraser, M.P., Upadhyay, N., Herckes, P., Sundblom, M., Lantz, J., Solomon, P.A., 2013. Characterization of summertime coarse particulate matter in the Desert Southwest-Arizona, USA. J. Air Waste Manage. Assoc. 63, 764–772.
Corti, G., Sanjurio, M.J.F., Ugolini, F.C., 1998. Randomly interstratified kaolinite-smectite from Galicia (NW Spain): a new procedure for determination. Clay Clay Miner. 46, 705–711.
Crouvi, O., Pelletier, J.D., Rasmussen, C., 2013. Predicting the thickness and aeolian fraction of soils in upland watersheds of the Mojave Desert. Geoderma 195–196, 94–110.
Dahlgren, R.A., Boettinger, J.L., Huntington, G.L., Amundson, R.G., 1997. Soil development along an elevational transect in the western Sierra Nevada, California. Geoderma 78, 207–236.
Dahms, D.E., 1993. Mineralogical evidence for eolian contribution to soils of late Quaternary moraines, Wind River Mountains, Wyoming, USA. Geoderma 59, 175–196.
Dickinson, W.R., 1991. Tectonic setting of faulted Tertiary strata associated with the Catalina core complex in southern Arizona. Geol. Soc. Am. Spec. Pap. 264 (Boulder, CO.).
Dickinson, W.R., 2002. The Basin and Range province as a composite extensional domain. Int. Geol. Rev. 44, 1–38. http://dx.doi.org/10.2747/0020-6814.44.1.1.
Dixon, J.L., Heimsath, A.M., Amundson, R., 2009. The critical role of climate and saprolite weathering in landscape evolution. Earth Surf. Process. Landf. 34, 1507–1521.
Dixon, J.L., Hartshorn, A.S., Heimsath, A.M., DiBiase, R.A., Whipple, K.X., 2012. Chemical weathering response to tectonic forcing: a soils perspective from the San Gabriel Mountains, California. Earth Planet. Sci. Lett. 323-324, 40–49.
Downs, R.T., Hall-Wallace, M., 2003. The American mineralogy crystal structure database. Am. Mineral. 88, 247–250.
Eberl, D., 2003. User's Guide to ROCKJOCK-a Program for Determining Quantitative Mineralogy from Powder X-Ray Diffraction Data.
Egli, M., Mirabella, A., Sartori, G., Fitze, P., 2003. Weathering rates as a function of climate: results from a climosequence of the Val Genova (Trentino, Italian Alps). Geoderma 111, 99–121.
Ferrier, K.L., Kirchner, J.W., Finkel, R.C., 2011. Estimating millennial-scale rates of dust incorporation into eroding hillslope regolith using cosmogenic nuclides and immobile weathering tracers. J. Geophys. Res. 116 (F03022).
Gilkes, R.J., Suddhiprakarn, A., Armitage, T.M., 1980. Scanning electron microscope morphology of deeply weathered granite. Clay Clay Miner. 28, 29–34.
Goudie, A.S., Viles, H.A., 2012. Weathering and the global carbon cycle: geomorphological perspectives. Earth Sci. Rev. 113, 59–71.
Graham, R.C., O'Geen, A.T., 2010. Soil mineralogy trends in California landscapes. Geoderma 154, 418–437.
Hahnenberg, M., Nicoll, K., 2014. Geomorphic and land cover identification of dust sources in the eastern Great Basin of Utah, U.S.A. Geomorphology 204, 657–672.
Hattar, B.I., Taimeh, A.Y., Ziadat, F.M., 2010. Variation in soil chemical properties along toposequences in an arid region of the Levant. Catena 83, 34–45.
Hirmas, D.R., Graham, R.C., 2011. Pedogenesis and soil-geomorphic relationships in an Arid Mountain Range, Mojave Desert, California. Soil Sci. Soc. Am. J. 75, 192–206.
Huggett, R.J., 1975. Soil landscape systems: a model of soil genesis. Geoderma 13, 1–22.
Jackson, M.L., 1963. Interlayering of expansible layer silicates in soils by chemical weathering. Clay Clay Miner. 11, 29–46.
Jackson, M.L., 1965. Clay transformations in soil genesis during the Quaternary. Soil Sci. 99, 15–22.
Jeong, G.Y., 2000. The dependence of localized crystallization of halloysite and kaolinite on primary minerals in the weathering profile of granite. Clay Clay Miner. 48, 196–203.
Jeong, G.Y., Kim, Y., Chang, S., Kim, S.J., 2003. Morphological change of halloysite derived from weathering of illite in residual kaolin. Neues Jahrb. Mineral. Monatshefte 9, 421–432.
Joussein, E., Petit, S., Churchman, J., Theng, B., Righi, D., Delvaux, B., 2005. Halloysite clay minerals-a review. Clay Miner. 40, 383–426.
Khomo, L., Hartshorn, A.S., Rogers, K.H., Chadwick, O.A., 2011. Impact of rainfall and topography on the distribution of clays and major cations in granitic catenas of southern Africa. Catena 87, 119–128.
Khomo, L., Bern, C.R., Hartshorn, A.S., Rogers, K.H., Chadwick, O.A., 2013. Chemical transfers along slowly eroding catenas developed on granitic cratons in southern Africa. Geoderma 202-203, 192–202.
Konen, M.E., Jacobs, P.M., Burras, C.L., Talaga, B.J., Mason, J.A., 2002. Equations for predicting soil organic carbon using loss-on-ignition for North Central U.S. Soils. Soil Sci. Soc. Am. J. 66, 1878–1881.
Lawrence, C.R., Neff, J.C., Farmer, G.L., 2011. The accretion of aeolian dust in soils of the San Juan Mountains, Colorado, USA. J. Geophys. Res. 116 (F02013).
Litaor, M.I., 1987. The influence of eolian dust on the genesis of alpine soils in the Front Range, Colorado. Soil Sci. Soc. Am. J. 51, 142–147.
Lybrand, R.A., 2014. The Effects of Climate and Landscape Position on Mineral Weathering and Soil Carbon Storage in the Santa Catalina Critical Zone Observatory of Southern Arizona. Ph.D. dissertation. Univ. of Arizona, Tucson.
Lybrand, R., Rasmussen, C., 2014. Linking soil element-mass-transfer to microscale mineral weathering across a semiarid environmental gradient. Chem. Geol. 381, 26–39.
Lybrand, R., Rasmussen, C., 2015. Quantifying climate and landscape position controls on soil development in semiarid ecosystems. Soil Sci. Soc. Am. J. 79, 104–116.
Malla, P.B., 2002. Vermiculites–chemistry, mineralogy, and applications. In: Dixon, J.B., Schulze, D.G. (Eds.), Soil Mineralogy with Environmental Applications, SSSA Series No. 7. Soil Science Society of America, pp. 501–529.
McFadden, L.D., 2013. Strongly dust-influenced soils and what they tell us about landscape dynamics in vegetated aridlands of the southwestern United States. Geol. Soc. Am. Spec. Pap. 500, 501–532.
McTainsh, G., Strong, C., 2007. The role of aeolian dust in ecosystems. Geomorphology 89, 39–54.
Moore, D.M., Reynolds, R.C.J., 1997. X-Ray Diffraction and the Identification and Analysis of Clay Minerals.
Muhs, D.R., 1982. The influence of topography on the spatial variability of soils in Mediterranean climates. In: Thorn, C.E. (Ed.), Space and Time in Geomorphology. George Allen and Unwin, pp. 269–284.
Muhs, D.R., Benedict, J.B., 2006. Eolian additions to late quaternary alpine soils, Indian peaks wilderness area, Colorado front range. Arct. Antarct. Alp. Res. 38, 120–130.
Muhs, D.R., Budahn, J.R., Johnson, D.L., Reheis, M., Beann, J., Skipp, G., Fisher, E., Jones, J.A., 2008. Geochemical evidence for airborne dust additions to soils in Channel Islands National Park, California. GSA Bull. 120, 106–126.
Nettleton, W.D., Flach, K.W., Borst, G., 1968. A toposequence of soils in a tonalite grus in the southern California Peninsular Range. Soil Surv. Investig. Rep. 21.
Oh, N.-H., Richter, D.D., 2005. Elemental translocation and loss from three highly weathered soil-bedrock profiles in the southeastern United States. Geoderma 126, 5–25.
Papoulis, D., Tsolis-Katagas, P., Katagas, C., 2004. Progressive stages in the formation of kaolin minerals of different morphologies in the weathering of plagioclase. Clay Clay Miner. 52, 275–286.
Parfitt, R.L., Russell, M., Orbell, G.E., 1983. Weathering sequence of soils from volcanic ash involving allophane and halloysite, New Zealand. Geoderma 29, 41–57.
Porder, S., Hilley, G.E., Chadwick, O.A., 2007. Chemical weathering, mass loss, and dust inputs across a climate by time matrix in the Hawaiian Islands. Earth Planet. Sci. Lett. 258, 414–427.
Rasmussen, C., Matsuyama, N., Dahlgren, R.A., Southard, R.L., Brauer, N., 2007. Soil genesis and mineral transformation across an environmental gradient on andesitic lahar. Soil Sci. Soc. Am. J. 71, 225–237.
Rasmussen, C., Dahlgren, D.A., Southard, R.J., 2010. Basalt weathering and pedogenesis across an environmental gradient in the southern Cascade Range, California, USA. Geoderma 154, 473–485.
Rasmussen, C., Brantley, S., Richter, D., Blum, A., Dixon, J., White, A.F., 2011. Strong climate and tectonic control on plagioclase weathering in granitic terrain. Earth Planet. Sci. Lett. 301, 521–530.
Rasmussen, C., McGuire, L., Dhakal, P., Pelletier, J.D., 2017. Coevolution of soil and topography across a semiarid cinder cone chronosequence. Catena 156, 338–352.
Reheis, M.C., 2006. A 16-year record of eolian dust in Southern Nevada and California, USA: controls on dust generation and accumulation. J. Arid Environ. 67, 487–520.
Reheis, M.C., Kihl, R., 1995. Dust deposition in southern Nevada and California, 1984–1989: relations to climate, source area, and source lithology. J. Geophys. Res. 100, 8893–8918.
Reheis, M.C., Goodmacher, J.C., Harden, J.W., McFadden, L.D., Rockwell, T.K., Shroba, R.R., Sowers, J.M., Taylor, E.M., 1995. Quaternary soils and dust deposition in southern Nevada and California. Geol. Soc. Am. Bull. 107, 1003–1022.
Reid-Soukup, D.A., Ulery, A.L., 2002. Smectites. In: Dixon, J.B., Schulze, D.G. (Eds.), Soil Mineralogy with Environmental Applications, Book Series No. 7. Soil Science Society of America, Madison, WI, pp. 467–499.
Reynolds, R.C., 1971. Clay mineral formation in an alpine environment. Clay Clay Miner. 19, 361–374.
Reynolds, R.L., Reheis, M., Yount, J., Lamothe, P., 2006. Composition of aeolian dust in natural traps on isolated surfaces of the central Mojave Desert-insights to mixing, sources, and nutrient inputs. J. Arid Environ. 66, 42–61.
Riebe, C.S., Kirchner, J.W., Granger, D.E., Finkel, R.C., 2001. Strong tectonic and weak climatic control of long-term chemical weathering rates. Geology 29, 511–514.
Riebe, C.S., Kirchner, J.W., Finkel, R.C., 2004. Erosional and climatic effects on long-term chemical weathering rates in granitic landscapes spanning diverse climate regimes. Earth Planet. Sci. Lett. 224, 547–562.
Rietveld, H.M., 1969. A profile refinement method for nuclear and magnetic structures. J. Appl. Crystallogr. 2, 65–71.
Robertson, I.D.M., Eggleton, R.A., 1991. Weathering of granitic muscovite to kaolinite and halloysite and of plagioclase-derived kaolinite to halloysite. Clay Clay Miner. 39,

113–126.
Sandler, A., 2013. Clay distribution over the landscape of Israel: from the hyper-arid to the Mediterranean climate regimes. Catena 110, 119–132.
Soil Survey Staff, 2004. Soil survey laboratory methods manual. In: Soil Survey Investigations Report No. 42, Version 4.0. Lincoln, NE.
Soil Survey Staff, 2009. Soil survey field and laboratory methods manual. In: Burt, R. (Ed.), Soil Survey Investigations Report No. 51, Version 1.0. U.S. Department of Agriculture, Natural Resources Conservation Service.
Sommer, M., Schlichting, E., 1997. Archetypes of catenas in respect to matter-a concept for structuring and grouping catenas. Geoderma 76, 1–33.
Southard, R.J., Southard, S.B., 1987. Sand-sized kaolinized feldspar pseudomorphs in a California Humult. Soil Sci. Soc. Am. J. 51, 1666–1672.
Speakman, S.A., 2013. An Introduction to Rietveld Refinement using PANalytical X'Pert HighScore Plus v2.2d.
Taboada, T., Garcia, C., 1999. Pseudomorphic transformation of plagioclases during the weathering of granitic rocks in Galicia (NW Spain). Catena 35, 291–302.
Takahashi, T., Dahlgren, R., van Susteren, P., 1993. Clay mineralogy and chemistry of soils formed in volcanic materials in the xeric moisture regime of northern California. Geoderma 59, 131–150.
Tazaki, K., 1976. Scanning electron microscopic study of formation of gibbsite from plagioclase. In: Papers of the Institute for Thermal Spring Research. 45. pp. 11–24.
Turpault, M.-P., Righi, D., Uterano, C., 2008. Clay minerals: precise markers of the spatial and temporal variability of the biogeochemical soil environments. Geoderma 147, 108–115.
Vazquez, F.M., 1981. Formation of gibbsite in soils and saprolites of temperate-humid zones. Clay Miner. 16, 43–52.
Wada, K., Aomine, S., 1966. Occurrence of gibbsite in weathering of volcanic materials at Kuroishibaru, Kumamoto. Soil Sci. Plant Nutr. 12, 151–157.
Watson, J.P., 1964. A soil catena on granite in southern Rhodesia. J. Soil Sci. 15, 238–250.
Weaver, R.M., Jackson, M.L., Syers, J.K., 1971. Magnesium and silicon activities in matrix solutions of montmorillonite-containing soils in relation to clay mineral stability. Soil Sci. Soc. Am. Proc. 35, 823–830.
Wells, S.G., Dohrenwend, J.C., McFadden, L.D., Turrin, B.D., Mahrer, K.D., 1985. Late Cenozoic landscape evolution on lava flow surfaces of the Cima volcanic field, Mojave Desert, California. Geol. Soc. Am. Bull. 96, 1518–1529.
West, A.J., Galy, A., Bickle, M., 2005. Tectonic and climatic controls on silicate weathering. Earth Planet. Sci. Lett. 235, 211–228.
White, A., Brantley, S., 1995. Chemical weathering rates of silicate minerals; an overview. Rev. Mineral. Geochem. 31, 1–22.
Whittaker, R., Niering, W., 1965. Vegetation of the Santa Catalina Mountains. Arizona: a gradient analysis of the south slope. Ecology 46, 429–452.
Whittaker, R.H., Buol, S.W., Niering, W.A., Havens, Y.H., 1968. A soil and vegetation pattern in the Santa Catalina Mountains, Arizona. Soil Sci. 105, 440–450.
Whittig, L.D., Allardice, W.R., 1986. X-ray diffraction techniques. In: Klute, A. (Ed.), Methods of Soil Analysis, Part 1: Physical and Mineralogical Methods. Soil Sci. Soc. Amer., pp. 331–362.
Yoo, K., Amundson, R., Heimsath, A.M., Dietrich, W.E., Brimhall, G.H., 2007. Integration of geochemical mass balance with sediment transport to calculate rates of soil chemical weathering and transport on hillslopes. J. Geophys. Res. 112 (F02013).
Young, R.A., 1993. The Rietveld Method. Oxford University Press, New York.
Yousefifard, M., Ayoubi, S., Jalalian, A., Khademi, H., Makkizadeh, M.A., 2012. Mass balance of major elements in relation to weathering in soils developed on igneous rocks in a semiarid region, Northwestern Iran. J. Mt. Sci. 9, 41–58.
Ziegler, K., Hsieh, J.C.C., Chadwick, O.A., Kelly, E.F., Hendricks, D.M., Savin, S.M., 2003. Halloysite as a kinetically controlled end product of arid-zone basalt weathering. Chem. Geol. 202, 461–478.